Chinese Chemical Letters 36 (2025) 110498

Contents lists available at ScienceDirect

Chinese Chemical Letters

journal homepage: www.elsevier.com/locate/cclet

Efficient synthesis of nano high-entropy compounds for advanced oxygen evolution reaction

Genxiang Wang[a,b,1], Linfeng Fan[b,1], Peng Wang[b], Junfeng Wang[a], Fen Qiao[a,*], Zhenhai Wen[b,*]

[a] School of Energy and Power Engineering, Jiangsu University, Zhenjiang 212013, China
[b] CAS Key Laboratory of Design and Assembly of Functional Nanostructures, and Fujian Provincial Key Laboratory of Materials and Techniques Toward Hydrogen Energy, Fujian Institute of Research on the Structure of Matter, Chinese Academy of Sciences, Fuzhou 350002, China

ARTICLE INFO

Article history:
Received 20 August 2024
Revised 19 September 2024
Accepted 23 September 2024
Available online 24 September 2024

Keywords:
High-entropy sulfides
High-entropy phosphides
Oxygen evolution reaction
Efficient synthesis
Nano structure

ABSTRACT

Developing efficient electrocatalysts for oxygen evolution reaction (OER) is imperative to enhance the overall efficiency of electrolysis systems and rechargeable metal-air batteries operating in aqueous solutions. High-entropy materials, featured with their distinctive multi-component properties, have found extensive application as catalysts in electrochemical energy storage and conversion devices. However, synthesizing nanostructured high-entropy compounds under mild conditions poses a significant challenge due to the difficulty in overcoming the immiscibility of multiple metallic constituents. In this context, the current study focuses on the synthesis of an array of nano-sized high entropy sulfides tailored for OER *via* a facile precursor pyrolysis method at low temperature. The representative compound, $FeCoNiCuMnS_x$, demonstrates remarkable OER performance, achieving a current density of 10 mA/cm^2 at an overpotential of merely 220 mV and excellent stability with constant electrolysis at 100 mA/cm^2 for over 400 h. The *in-situ* formed metal (oxy)hydroxide has been confirmed as the real active sites and its exceptional performance can be primarily attributed to the synergistic effects arising from its multiple components. Furthermore, the synthetic methodology presented here is versatile and can be extended to the preparation of high entropy phosphides, which also present favorable OER performance. This research not only introduces promising non-noble electrocatalysts for OER but also offers a facile approach to expand the family of nano high-entropy materials, contributing significantly to the field of electrochemical energy conversion.

The enduring energy and environmental crises underscore the critical need to progress electrochemical energy storage and conversion technologies [1–3]. Among these, the eco-friendly and sustainable rechargeable metal-air batteries and hydrogen production *via* water splitting hold immense potential to meet our daily energy needs and drive sustainable green chemical production [4–6]. However, the overall energy efficiency of these technologies is largely governed by the oxygen evolution reaction (OER), a pivotal half-reaction known for its high overpotential, which stems from the sluggish four-electron transfer processes [7,8]. Consequently, there is a strong desire, albeit a challenging one, to develop sophisticated electrocatalysts that can reduce the OER overpotential, thereby minimizing the inherent energy loss in these energy conversion technologies. Currently, highly efficient Ir/Ru-based noble-metal oxides can significantly reduce OER overpotential by lowering the energy barrier and enhancing reaction kinetics, and they are extensively employed as benchmark catalysts in this field [9,10]. Nevertheless, their rarity and high costs pose challenges to their widespread application. Accordingly, considerable research efforts have been directed towards exploring earth-abundant and high-performance OER catalysts [8,11–15].

Recently, high-entropy materials (HEMs), featured with their composition of at least five principal metal elements within a single-phase crystal structure, have emerged as promising candidates as efficient OER electrocatalysts [16–19]. The unique polyatomic structure of HEMs confers them with distinctive characters like high entropy, cocktail effects, sluggish diffusion and lattice distortion, which endows them with exceptional catalytic activity and structure stability, outperforming traditional materials [17,18,20]. Moreover, the expansive compositional versatility of HEMs provides a broad spectrum of possibilities for precision tuning of their electronic and geometric structures, thereby increasing intrinsic

* Corresponding authors.
E-mail addresses: fqiao@ujs.edu.cn (F. Qiao), wen@fjirsm.ac.cn (Z. Wen).
[1] These authors contributed equally to this work.

https://doi.org/10.1016/j.cclet.2024.110498
1001-8417/

active sites and refining OER catalytic performance. A variety of HEMs like alloys [21,22], oxides/oxyhydroxide [9,23–25], sulfides [26,27], and selenides [28], have been explored as OER electrocatalysts. Of notable significance is the recent rise of high-entropy metal sulfides (HESs), which have shown tremendous potential as OER catalysts due to their superior catalytic activity and remarkable durability, attributes that stem from the synergistic interaction of their multiple components [26,27,29–32].

As there exists immiscibility of multiple metallic constituents, there remains challenges to explore feasible strategies for preparing active nano high-entropy sulfides [26,33,34]. Initially, Hu *et al.* pioneered the preparation of $(CrMnFeCoNi)S_x$ nanoparticles as an OER catalyst using a pulse thermal decomposition method. The prepared HES nanoparticles achieved 100 mA/cm^2 at an overpotential of just 295 mV and impressive stability in alkaline medium [26]. Since then, several cases of HESs with different metal components has been developed *via* various synthetic method such as high-energy planetary ball-milling process [35], solvothermal method [27], cation exchange strategy [36], and thermal decomposition of mixture of metal dithiocarbamate precursors [37]. For instance, Nguyenn *et al.* developed a series of sulfate-containing high-entropy sulfides using a two-step solvothermal method, of which, the sulfate-containing $FeNiCoCrMnS_2$ presented excellent OER activity with an overpotential of only 199 mV to reach 10 mA/cm^2 and maintained stable electrolysis for 55 h at a current density of 500 mA/cm^2 [27]. Qu *et al.* achieved preparation of bulk HES, *i.e.*, $(MoWReMnCr)S_2$, *via* thermal decomposition of mixture of metal dithiocarbamate precursors. The resulting two-dimensional (2D) HES nanosheets, derived from exfoliating the bulk $(MoWReMnCr)S_2$ was applied as electrocatalysts for OER, requiring 229 mV to deliver a current density of 10 mA/cm^2 [37]. The studies highlighted have shown the tremendous promise of HESs as efficient OER catalysts. Even so, some of the above methods require multi-step processes [36], specialized equipment and stringent conditions [26,31] to obtain nano HESs. Therefore, there exists significant scope for further developing more facile, readily scalable and universally applicable synthetic methods for preparing active nano high-entropy sulfides.

Herein, we developed a series of high-entropy sulfides *via* a facial precursor pyrolysis method that is also adapted to preparing high-entropy phosphides. Both the synthesized high-entropy sulfides and phosphides present favorable OER performance, of which, the representative $FeCoNiCuMnS_x$ with a nano three-dimensional cross-linked structure, showcases a low overpotential of 220 mV at 10 mA/cm^2 and exceptional stability without observable degradation during an over 400 h durability test at 100 mA/cm^2. This impressive performance of $FeCoNiCuMnS_x$ can be primarily attributed to the synergistic effects arising from its multiple components. The developed facile synthetic method and the investigation of OER performance of these prepared high-entropy catalysts offer a platform for the advancement of high-entropy electrocatalysts.

The representative $FeCoNiCuMnS_x$ HES was prepared *via* a one-step pyrolyzing mixture of metal complexes precursor at a low temperature of 500 °C (Fig. 1a). The X-ray diffraction (XRD) pattern shows that the predominant diffraction peaks of $FeCoNiCuMnS_x$ correspond to the (111), (220), (311), (400), (422) and (440) planes of its crystal structure, conforming to similar crystal structure of Co_3S_4 (PDF #75–1561). Notably, three additional quinary HESs with same crystalline phase as $FeCoNiCuMnS_x$, *i.e.*, $FeCoNiCrZnS_x$, $FeCoNiCrCuS_x$, and $FeCoNiCuZnS_x$, were also successfully synthesized by altering the metal ions during the synthetic process (Fig. 1b). Not limited that, such synthetic routine can also be extended to prepare a series of high-entropy phosphides (HEPs) including $FeCoNiCrCuP_x$, $FeCoNiCuZnP_x$, $FeCoNiCuMnP_x$, and $FeCoNiCrMnP_x$, simply by substituting thiourea with tri-*n*-octylphosphine in the precursor. The XRD patterns of these phosphides show major diffraction peaks corresponding to the (111), (201), (210) and (300) planes, aligning with those of Ni_2P (PDF #03–0953) (Fig. 1c) [38], suggesting the formation of single-phase structure in these HEPs.

The morphology of $FeCoNiCuMnS_x$ was firstly examined by scanning electron microscopy (SEM). SEM images reveal that $FeCoNiCuMnS_x$ exhibits three-dimensional (3D) crosslinked structure consist of randomly distributed nano branches (Figs. 2a-c). Transmission electron microscope (TEM) image further confirms the crosslinked nano branches structure of $FeCoNiCuMnS_x$ (Fig. 2d). High-resolution TEM (HRTEM) identifies interplanar spacings of around 0.283 nm, corresponding to the (311) lattice plane of $FeCoNiCuMnS_x$ (Fig. 2e). Notably, HRTEM image analysis on the $FeCoNiCuMnS_x$ further verifies the presence of amorphous carbon at the periphery of the nano branches structure, which originates from the pyrolysis of coordinated ammonium citrate (Fig. S1 in Supporting information). In addition, the selected area electron diffraction (SAED) pattern shows that the lattice planes derived from the diffraction rings correspond well with the XRD pattern of $FeCoNiCuMnS_x$ (Fig. 2f). Scanning TEM energy dispersive X-ray spectroscopy (STEM-EDX) elemental mapping shows uniform distribution of Fe, Co, Ni, Cu, Mn, S throughout the

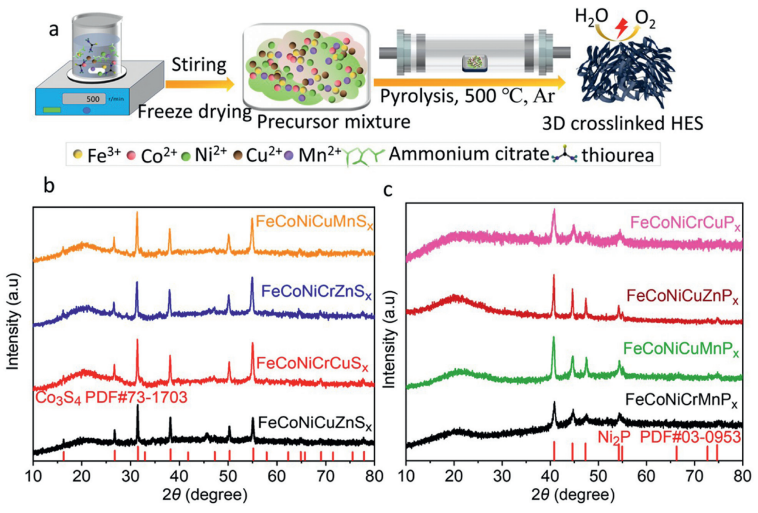

Fig. 1. (a) Schematic illustration for the synthetic process of $FeCoNiCuMnS_x$. XRD patterns of prepared HESs (b) and HEPs (c).

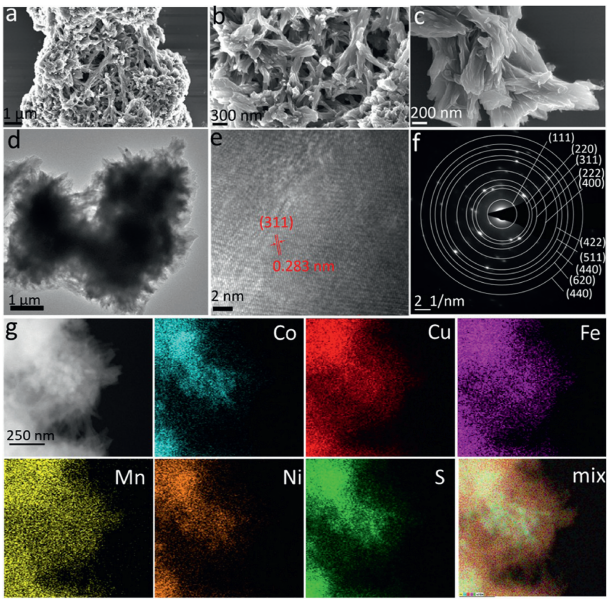

Fig. 2. Structural and morphological characterization of $FeCoNiCuMnS_x$. (a-c) SEM images at various magnifications, (d) TEM image, (e) high-resolution TEM image, (f) SAED pattern, (g) high-angle annular dark-field scanning transmission electron microscopy (HAADF-STEM) image with its corresponding elemental mapping images.

structure, further confirming the single-phase nature of the prepared HES (Fig. 2g). Moreover, the accurate atomic molar ratio of Fe, Co, Ni, Cu and Mn in $FeCoNiCuMnS_x$ was determined to be 17.26:22.10:21.60:18.20:20.84 by using inductively coupled plasma optimal emission spectroscopy (ICP-OES) (Fig. S2a in Supporting information). The similar ratio of various metallic elements further verifies the high-entropy nature of $FeCoNiCuMnS_x$. Furthermore, the morphologies of the other three HESs and the prepared HEPs were also revealed by SEM and TEM techniques, which show the other prepared HESs present similar morphologies with $FeCoNiCuMnS_x$ (Fig. S3 in Supporting information), while the HEPs display a structure with small nanoparticles anchored on carbon nanobelt (Figs. S4 and S5 in Supporting information).

X-ray photoelectron spectroscopy (XPS) technique was then performed to analyze the chemical composition and valence states of the $FeCoNiCuMnS_x$ surface (Fig. S6 in Supporting information and Fig. 3). The survey spectrum confirms the existent of Fe, Co, Ni, Cu, Mn and S on the surface (Fig. S6a). The high-resolution XPS spectra of Fe 2p can be split into six peaks (Fig. 3a). Those at 719.8 eV, 709.2 eV, 705.4 eV can be attributed to Fe^{2+} species, while the peaks at 723.5 eV and 712.5 eV are assigned to the Fe^{3+} species of Fe $2p_{1/2}$ and Fe $2p_{3/2}$, respectively, with a satellite peak at 716.1 eV [39,40]. For Co 2p, two pairs of peaks (796.2 eV and 781.3 eV) and (798.9 eV and 785.6 eV) can be assigned to Co^{3+} and Co^{2+} species of Co $2p_{1/2}$ and Co $2p_{3/2}$, respectively (Fig. 3b) [41,42]. The Ni 2p spectrum predominantly features Ni^{3+} with binding energy of 857.7 eV, 861.1 eV, and 876.5 eV, alongside smaller signals indexed to Ni^{2+} (854.1 eV) and Ni^0 (851.0 eV) (Fig. 3c) [39,43]. The Cu 2p spectrum indicates the coexistence of Cu^+ (932.2 eV and 951.7 eV) and Cu^{2+} (935.6 eV and 953.7 eV) species Fig. 3d) [44]. Besides, the Mn species also present in mixed valence, with binding energies of 642.1 eV and 650.0 eV assigned to Mn^{2+} ions, and 645.7 eV and 653.8 eV assigned to Mn^{3+} ions (Fig. 3e) [26,27,45]. As for the S 2p spectrum, the peak located at 163.0 eV can be indexed to the presence of S_2^{2-}, and the peaks located at 167.8 eV can be assigned to SO_x^{2-} (Fig. 3f) [46,47], suggesting partial oxidation of surface sulfur species upon exposure to air.

The OER performance of the representative $FeCoNiCuMnS_x$ was evaluated in a three-electrode system in 1.0 mol/L KOH aqueous solution at room temperature. The catalyst powders mixed with some conductive carbons supported on Ni foam (NF) serve as the working electrodes (Supporting information). For comparison, apart from the commercial reference IrO_2 and the used substrates, the controlled quaternary ($FeCoNiCuS_x$), ternary ($FeCoNiS_x$), and binary ($FeNiS_x$) sulfides were also prepared using the similar method by only reducing metallic species (Figs. S7–S9 in Supporting information). Fig. 4a shows the linear sweep voltammetry (LSV) profiles for the series of electrodes. The $FeCoNiCuMnS_x$ demonstrates the lowest overpotential of 220 mV to delivery 10 mA/cm^2, outperforming those of $FeCoNiCuS_x$ (259 mV), $FeCoNiS_x$ (273 mV), $FeNiS_x$ (298 mV) and even the commercial IrO_2 (317 mV). Moreover, $FeCoNiCuMnS_x$ also presents superior catalytic activity at higher current density. The overpotentials for delivering a cur-

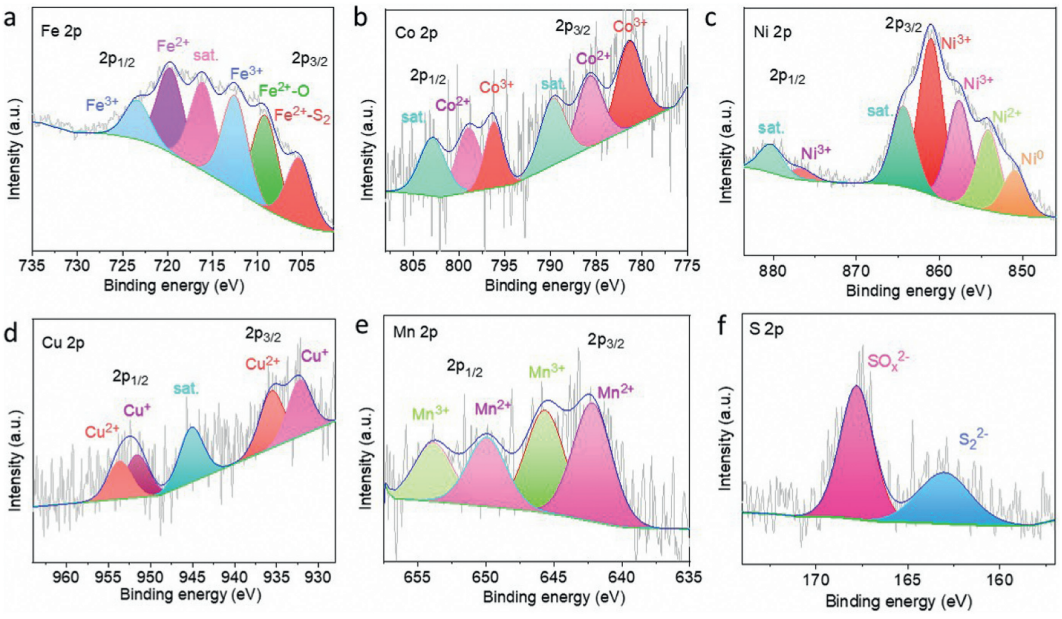

Fig. 3. High-resolution XPS spectra of Fe 2p (a), Co 2p (b), Ni 2p (c), Cu 2p (d), Mn 2p (e), S 2p (f) in $FeCoNiCuMnS_x$.

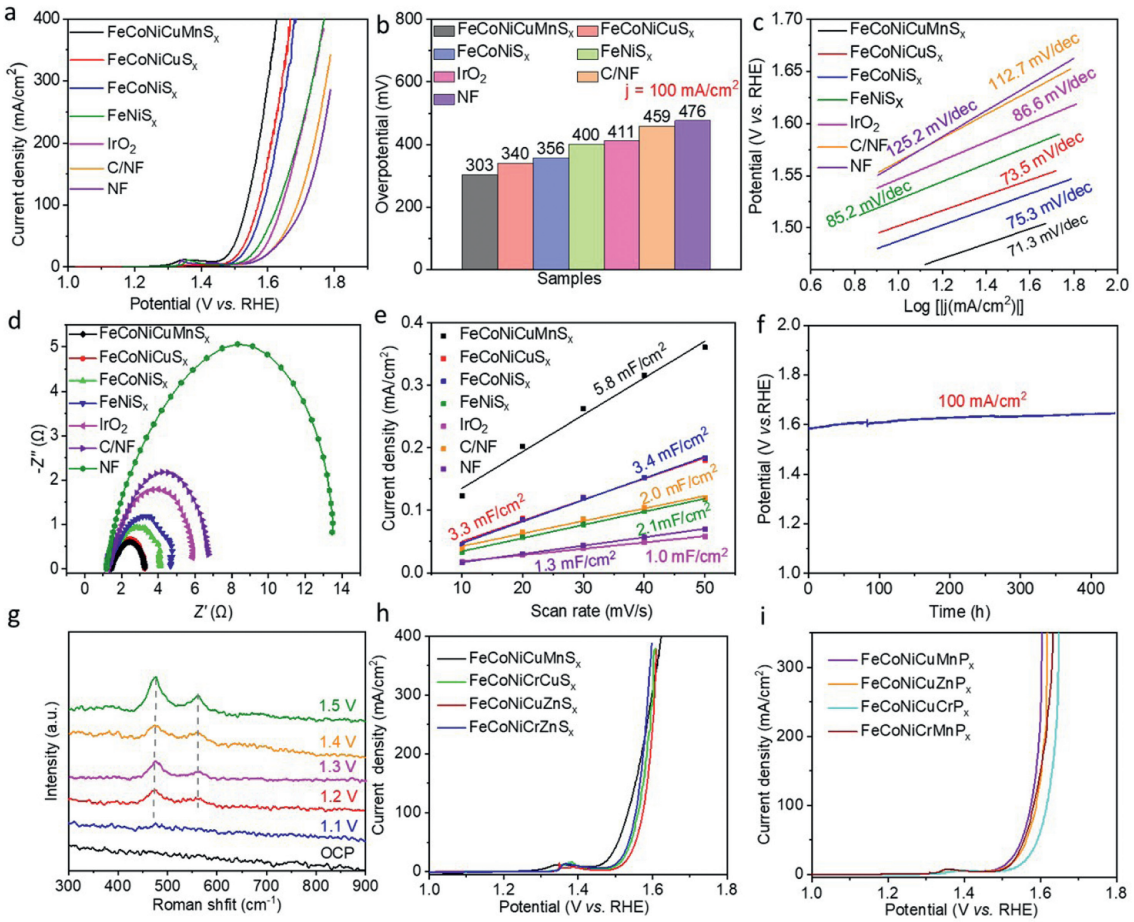

Fig. 4. Electrochemical OER performance of the $FeCoNiCuMnS_x$ and these controlled samples. (a) LSV curves with 85% IR correct collected at 1 mV/s. (b) Comparison of overpotentials at current density of 100 mA/cm^2. (c) Tafel slopes. (d) EIS spectra measured at 1.52 V *vs.* RHE. (e) The slop corresponding to the specific capacitance in the non-Faradaic region (C_{dl}). (f) Chronopotentiometric curve of $FeCoNiCuMnS_x$ at 100 mA/cm^2. (g) *In-situ* Raman spectrum of $FeCoNiCuMnS_x$ tested at different potentials. LSV curves of different HESs (h) and HEPs (i).

rent density of 100 mA/cm^2 were summarized in Fig. 4b, which shows that only 303 mV is required for the $FeCoNiCuMnS_x$, significantly lower than the controlled samples, indicating a synergistic effect from multiple metallic active sites on improving OER performance. The OER performance of $FeCoNiCuMnS_x$ is comparable to that of other reported HESs (Table S1 in Supporting information) [26,27,30,35,36,39,41,48]. The reaction kinetics of these catalysts were assessed by the Tafel slopes calculated from the LSV curves in Fig. 4a. The prepared HES possesses a Tafel slope value of 71.3 mV/dec, lower than all these controlled samples, suggesting its faster reaction kinetics of OER (Fig. 4c). The kinetics were further revealed by the electrochemical impedance spectroscopy (EIS) test. The Nyquist plots in Fig. 4d show a decrease in the charge-transfer resistance (R_{ct}) with increasing element incorporation in the catalysts, and the $FeCoNiCuMnS_x$ has the smallest semicircle diameter, indicating the fastest charge transfer rate at the $FeCoNiCuMnS_x$ catalytic interface and confirming its superior OER kinetic. Then the electrochemical surface areas (ECSAs) of these samples were estimated based on the double-layer capacitance (C_{dl}) values, which are proportional to ECSAs (Fig. S10 in Supporting information). The largest C_{dl} value (5.8 mF/cm^2) of $FeCoNiCuMnS_x$ compared with controlled samples manifests its more active sites for catalytic reaction (Fig. 4e).

In addition, the durability of the $FeCoNiCuMnS_x$ was checked by chronopotentiometric (CP) tests. The $FeCoNiCuMnS_x$ can maintain constant potential (around 1.45 V *versus* reversible hydrogen electrode (*vs.* RHE)) at 10 mA/cm^2 for 24 h without degradation, as evidenced by the nearly overlapping LSV curves and unchanged XRD patterns before and after the stability test (Fig. S11 in Supporting information). Moreover, stability at higher current density was also performed to evaluate its potential application in practice. As shown in Fig. 4f, the $FeCoNiCuMnS_x$ can maintain stable electrolysis at 100 mA/cm^2 for >400 h. Then the morphology and surface valent state of elements post-CP test were analyzed by SEM and XPS techniques, which shows no obvious morphology change but presents significant increase in higher oxidation state of metallic elements and sulfur element (Figs. S12 and S13 in Supporting information), suggesting oxidation occurred on the surface of $FeCoNiCuMnS_x$ after OER. The surface oxidation phenomenon was further revealed by the *in-situ* Raman spectra. Fig. 4g shows that there is no obvious peak at open circuit potential (OCP) within the tested range. When the input voltage increased to 1.2 V *vs.* RHE, dual evident peaks appeared at 476 cm^{-1} ($\delta(M^{III}\text{-}O)$) and 562 cm^{-1} ($\nu(M^{III}\text{-}O)$), which can be identified as the A_{1g} stretching vibration and e_g bending modes of the *in-situ* formed metal (oxy)hydroxid (MOOH), respectively [27,41,49,50]. The above results confirm surface reconstruction of $FeCoNiCuMnS_x$ during OER process, just as the previous reports that metal chalcogenides act as pre-catalysts for oxidation reaction, and metal (oxy)hydroxide are the true active sites, applicable to high-entropy materials as well [27]. Additionally, the OER performance of other quintuple high-entropy sulfides and phosphides were also preliminarily investigated under similar conditions, which shows that the other three HESs perform as well

as the $FeCoNiCuMnS_x$ for OER (Fig. 4h), and the $FeCoNiCuMnP_x$ with the best activity among these prepared phosphides achieves 10 mA/cm^2 at an overpotential of 260 mV, a little inferior to the prepared sulfides (Fig. 4i). Remarkably, the OER performance of these prepared high-entropy sulfides and phosphides are comparable with these reported outstanding ones (Table S1 in Supporting information).

In summary, a range of high-entropy sulfides and phosphides with favorable catalytic activity for OER were successfully synthesized by a facile precursor pyrolysis method at low temperature. The physicochemical properties of the representative $FeCoNiCuMnS_x$ for OER was thoroughly investigated. $FeCoNiCuMnS_x$, featuring a nano three-dimensional cross-linked structure, demonstrates superior catalytic activity with a low overpotential of 220 mV to deliver 10 mA/cm^2 and maintains stable electrolysis at 100 mA/cm^2 for over 400 h. Based on a series of experimental characterizations, the *in-situ* formed metal (oxy)hydroxide during the OER process was confirmed to be the real active sites, and the good OER performance can be primarily attributed to the synergistic effects arising from its multiple components. This work not merely introduces superior nano electrocatalysts for OER, but also provides a gentle and universal approach for expanding the family of nano high-entropy compounds, significantly contributing to the development of electrochemical energy storage and conversion technologies.

Declaration of competing interest

The authors declare that they have no known competing financial interests or personal relationships that could have appeared to influence the work reported in this paper.

CRediT authorship contribution statement

Genxiang Wang: Writing – original draft, Funding acquisition, Conceptualization. **Linfeng Fan:** Methodology, Investigation, Data curation. **Peng Wang:** Validation, Methodology. **Junfeng Wang:** Supervision. **Fen Qiao:** Writing – review & editing, Supervision. **Zhenhai Wen:** Writing – review & editing, Funding acquisition, Conceptualization.

Acknowledgments

This work was financially supported by the National Natural Science Foundation of China (Nos. 22209183, 22225902, U22A20436), and the Advanced Talents of Jiangsu University, China (No. 23JDG027).

Supplementary materials

Supplementary material associated with this article can be found, in the online version, at doi:10.1016/j.cclet.2024.110498.

References

[1] G. Wang, J. Chen, Z. Wen, J. Li, Sci. China Mater. 67 (2024) 1791–1803.
[2] Y. Zhang, D. Wang, S. Wang, Small 18 (2022) e2104339.
[3] Z. Qi, Y. Zhou, R. Guan, Y. Fu, J.B. Baek, Adv. Mater. 35 (2023) 2210575.
[4] Y. Liang, Y. Yao, Nat. Rev. Mater. 8 (2022) 109–122.
[5] H. Wu, Z. Li, Z. Wang, et al., Appl. Catal. B: Environ. 325 (2023) 122356.
[6] I. Roger, M.A. Shipman, M.D. Symes, Nat. Rev. Chem. 1 (2017) 0003.
[7] Z. Hou, C. Cui, Y. Li, et al., Adv. Mater. 35 (2023) 2209876.
[8] S. Kaushik, X. Xiao, Q. Xu, EnergyChem 5 (2023) 100104.
[9] L. Zhang, W. Cai, N. Bao, H. Yang, Adv. Mater. 34 (2022) e2110511.
[10] X. Huo, H. Yu, B. Xing, X. Zuo, N. Zhang, Chem. Rec. 22 (2022) e202200175.
[11] J. Li, R. Güttinger, R. Moré, et al., Chem. Soc. Rev. 46 (2017) 6124–6147.
[12] X. Guo, K. Yue, J. Zheng, et al., Mater. Chem. Front. 7 (2023) 3728–3737.
[13] X. Yin, Y. Hua, Z. Gao, Renewables 1 (2023) 190–226.
[14] W. Shen, J. Liu, G. Wen, et al., Chin. Chem. Lett. (2024), doi:10.1016/j.cclet.2024.110184.
[15] Y. Yang, R. Su, D. Wang, et al., Renewables 2 (2024) 250–263.
[16] J.W. Yeh, S.K. Chen, S.J. Lin, et al., Adv. Eng. Mater. 6 (2004) 299–303.
[17] J.W. Yeh, S.J. Lin, J. Mater. Res. 33 (2018) 3129–3137.
[18] Y. Ma, Y. Ma, Q. Wang, et al., Energy Environ. Sci. 14 (2021) 2883–2905.
[19] Y. Cui, Y. Zhang, Z. Cao, et al., SusMat 2 (2022) 65–75.
[20] S. Schweidler, M. Botros, F. Strauss, et al., Nat. Rev. Mater. 9 (2024) 266–281.
[21] H. Zhu, S. Sun, J. Hao, et al., Energy Environ. Sci. 16 (2023) 619–628.
[22] R. He, L. Yang, Y. Zhang, et al., Energy Storage Mater. 58 (2023) 287–298.
[23] C. Feng, Y. Zhou, M. Chen, et al., Appl. Catal. B: Environ. 349 (2024) 123875.
[24] H. Xu, Y. Hu, X. Lin, et al., Appl. Surf. Sci. 633 (2023) 157624.
[25] F. Wang, P. Zou, Y. Zhang, et al., Nat. Commun. 14 (2023) 6019.
[26] M. Cui, C. Yang, B. Li, et al., Adv. Energy Mater. 11 (2021) 2002887.
[27] T.X. Nguyen, Y.H. Su, C.C. Lin, J.M. Ting, Adv. Funct. Mater. 31 (2021) 2106299.
[28] F. Qian, L. Peng, D. Cao, et al., Joule 8 (2024) 1–15.
[29] L. Wu, X. Shen, Z. Ji, et al., Adv. Funct. Mater. 33 (2022) 2208170.
[30] M. Guo, P. Li, A. Wang, et al., Chem. Commun. 59 (2023) 5098–5101.
[31] Y. Liao, R. Zhu, W. Zhang, et al., Nano Res. 17 (2023) 3379–3389.
[32] J. Chen, K. Wang, Z. Liu, et al., Chem. Eng. J. 489 (2024) 151234.
[33] Y. Yao, Z. Huang, P. Xie, et al., Science 359 (2018) 1489–1494.
[34] Z. Wang, J. You, Y. Zhao, et al., J. Environ. Chem. Eng. 11 (2023) 109080.
[35] L. Lin, Z. Ding, G. Karkera, et al., Small Struct. 4 (2023) 2300012.
[36] Y. Lei, L. Zhang, W. Xu, Nano Res. 15 (2022) 6054–6061.
[37] J. Qu, A. Elgendy, R. Cai, et al., Adv. Sci. 10 (2023) e2204488.
[38] C. Tang, R. Zhang, W. Lu, et al., Angew. Chem. Int. Ed. 129 (2017) 860–864.
[39] Y. Zhao, J. You, Z. Wang, et al., Int. J. Hydrogen Energy 70 (2024) 599–605.
[40] Z. Yu, D.W. Boukhvalov, H. Tan, et al., Chem. Eng. J. 494 (2024) 153094.
[41] J. Shi, H. Jiang, X. Hong, J. Tang, Appl. Surf. Sci. 642 (2024) 158598.
[42] T. Zhang, Y.L. Meng, Y.H. Zhao, et al., Chem. Commun. 58 (2022) 7682–7685.
[43] B.C. Moon, W.H. Choi, K.H. Kim, et al., Small 15 (2019) e1804764.
[44] K. Gu, X. Zhu, D. Wang, et al., J. Energy Chem. 60 (2021) 121–126.
[45] R. Nandan, G. Raj, K.K. Nanda, ACS Appl. Mater. Interfaces 14 (2022) 16108–16116.
[46] W. Cheng, J. Liu, J. Hu, et al., Small 19 (2023) 2301915.
[47] P. Wang, G. Wang, K. Chen, et al., Nano Energy 118 (2023) 108992.
[48] S. Li, L. Tong, Z. Peng, B. Zhang, X. Fu, Green Chem. 26 (2024) 384–395.
[49] Z. Jiang, Y. Yuan, L. Tan, M. Li, K. Peng, Appl. Surf. Sci. 627 (2023) 157282.
[50] L. Fan, Y. Ji, G. Wang, et al., J. Am. Chem. Soc. 144 (2022) 7224–7235.